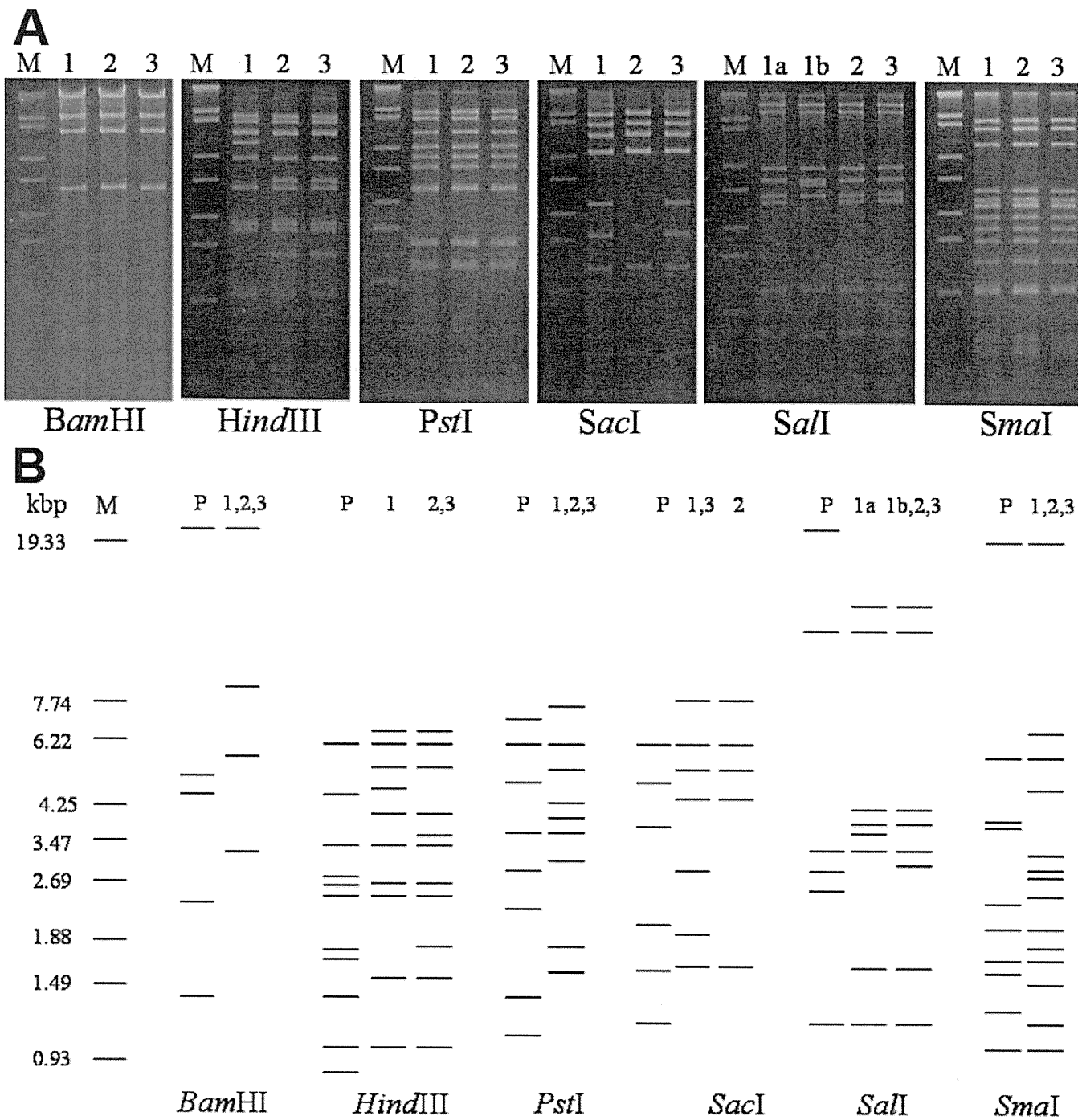

Figure 1. Restriction patterns of strains number 1–9. **A**: Restriction patterns of 9 strains isolated in 1986, 1991, and 1996. Lane M: molecular weight marker (lambda DNA digested with EcoT14I). Lane 1: representative strains number 1–3 isolated in 1986. Lanes 1a and 1b represent the two kinds of restriction patterns for SalI (HAdV-8A and HAdV-8B). Lane 2: representative strains number 4–6 isolated in 1991 (HAdV-8K). Lane 3: representative strains number 7–9 isolated in 1996 (HAdV-8E). **B**: Schematic presentation of the restriction patterns of strains number 1–9 and HAdV-8 prototype.

11were in HAdV-54 (data not shown). Strains of number 10 and 11 were reclassified as HAdV-54.

DNA restriction enzyme analysis: After restriction enzyme digestion, the 11 strains were electrophoresed in two gels. Strains of number 1 to 9 isolated in 1986, 1991, and 1996 that reacted strongly to HAdV-8 antiserum were run in one gel (Figure 1A). The remaining 2 strains of number 10 and 11 isolated in 2003 showing weak reaction to HAdV-8 antiserum were run in another gel (Figure 2A). To make the restriction patterns of these strains are easy to read, they were also shown

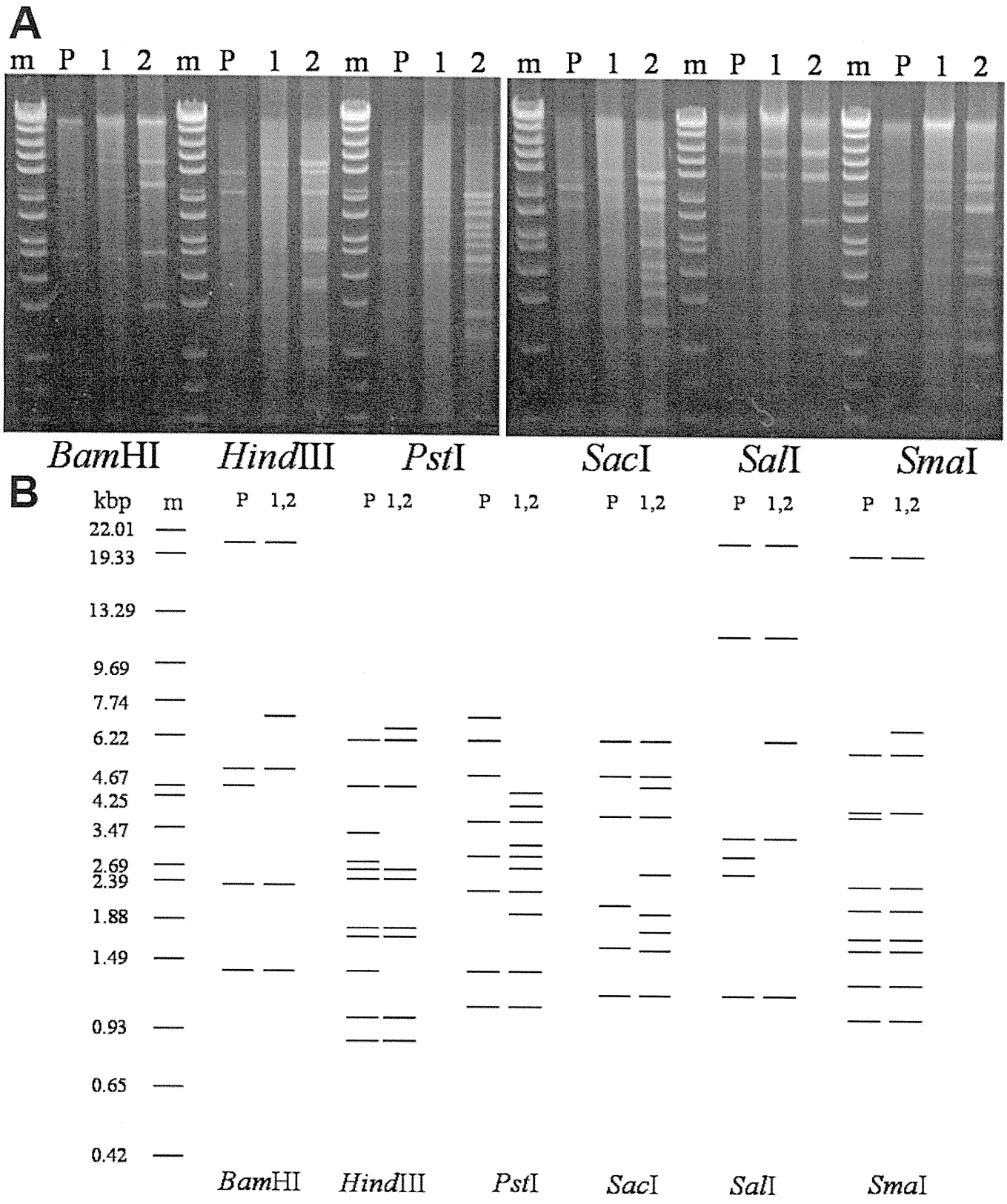

Figure 2. Restriction patterns of strains number 10 and 11. **A**: Restriction patterns of 2 strains isolated in 2003. Lane m: molecular weight marker (lambda DNA digested with EcoT14I plus BglII). Lane P: HAdV-8 prototype. Lane 1: representative strains number 10 isolated in Itoman in 2003 (HAdV-54). Lane 2: representative strains number 11 isolated in Matsuyama in 2003 (HAdV-54). **B**: Schematic presentation of the restriction patterns of strains HAdV-8 prototype and samples number 10 and 11.

as schematic presentations (Figure 1B and Figure 2B). It was revealed that the 11 strains analyzed in this study were divided into five genome types according to the profile of restriction patterns (Table 1). All of 11 strains showed different restriction patterns from those of the HAdV-8 prototype. Of the 3 strains isolated in 1986, number 1 showed restriction patterns similar to HAdV-8A and number 2 and 3 were similar to HAdV-8B. number 4 to 6 isolated in 1991, and number 7 to 9 isolated in 1996 showed identical restriction patterns with restriction endonucleases BamHI, HindIII, PstI, SalI, and SmaI. With SacI, the strains number 4 to 6 isolated in 1991 exhibited different patterns from those of the strains isolated in 1996 and any other previously known HAdV-8 genome types. This new pattern revealed a new genome type of HAdV-8 that we designated as HAdV-8K in accordance with the serial studies in the Asia Pacific area. The restriction patterns of strains number 7 to 9 isolated in 1996 corresponded to HAdV-8E. The restriction patterns of strains number 10 and 11 isolated in 2003 were similar to those of HAdV-54. The results of DNA restriction enzyme analysis are summarized in Table 1.

DISCUSSION

To investigate the genetic characteristics of HAdV-8 isolates and their chronological pattern, we demonstrated the molecular biologic characteristics of 11 HAdV strains isolated from sporadic cases of EKC in Japan over an 18-year period in the present study. All of the strains were identified as HAdV-8 by the neutralization method. In the present study, a new variant strain, HAdV-8K, was identified by the DNA restriction method. The DNA restriction method for genome typing identified two strains isolated in 2003 as HAdV-54, not HAdV-8. These were also confirmed as HAdV-54 by phylogenetic analysis of partial hexon gene. HAdV-54 was not detected before the early 1990s, but replaced HAdV-8 in Japan in the 2000s [21]. HAdV-54 in samples collected in 2003 is consistent with that study. However, major causes of EKC vary in different countries, and HAdV-8 is still the most common pathogenic virus in the Middle East [22].

As HAdV-8 has a much higher tropism for conjunctival cells and produces more severe clinical manifestations and pathological alterations in EKC than HAdV-19 or HAdV-37, HAdV-8 has been the target of extensive study [10]. After HAdV-8 was first isolated as an etiology of EKC, many HAdV-8 genome types have been identified by applying restriction endonucleases and cleavage pattern analysis [7]. Distinct nomenclature systems have been used for these genome types. A nomenclature system using a numerical code to denote adenovirus genome types has been proposed, and HAdV-8/D1 to HAdV-8/D12 have been described depending on the chronological order of the respective isolates [11-13]. Another nomenclature system was also proposed in which HAdV-8 genome types are denoted by alphabetical order [5]. According to the nomenclature system, HAdV-8 genome types are classified as HAdV-8A to HAdV-8K [5-7,10,23]. Although both systems are commonly used, we adopted the latter nomenclature system here in accordance with a series of collaborative studies of HAdV-8. We compared the restriction patterns of the strains in this study with those of all previously known genome types of HAdV-8. One new genome type was discovered and designated as HAdV-8K.

The cleavage patterns of 2 strains isolated in 2003 with any of the 6 restriction endonucleases were different from those of any other previously known genome type of HAdV-8. The unique restriction patterns indicated that an uncommon mutation or recombination event might have occurred. The restriction patterns of these 2 strains were consistent with those of HAdV-54, which was first reported in 2008 [14]. Furthermore, these strains were neutralized weakly by the antiserum against HAdV-8. Similarly, HAdV-54 responds weakly to the antiserum for HAdV-8. Because of the absence of serotype specific antiserum, the weak reaction with the antiserum against HAdV-8 might be a clue for detecting HAdV-54 at the current time. The strains of number 10 and 11 were also confirmed as HAdV-54 by phylogeny-based classification, which is an effective tool for the rapid identification of HAdVs.

Although HAdV-8 seems to display considerable variability and adenoviral ocular infection is common in East Asian countries, few studies on the circulation of HAdV-8 genome types have been reported in Japan. Thus, this is a report even more focused on the genetic characteristics of HAdV-8 isolates and their chronological patterns than the analysis of a new genome type. Two studies reported the isolation of HAdV-8A and HAdV-8B in Sapporo [5], and the circulation of HAdV-8 genome types in Hiroshima over a 15-year period [10]. In this study, restriction endonuclease analyses revealed a new genome type, HAdV-8K, in Sapporo, where HAdV-8A and HAdV-8B are endemic. The strains isolated in 1986 were HAdV-8A and HAdV-8B, and HAdV-8K strains were isolated from samples collected in 1991. The strains isolated in 1996 exhibited a similar restriction pattern as that of HAdV-8E, which was first isolated in Kaohsiung, Taiwan [6]. HAdV-8 was reported as being prevalent in 1986, 1991, and 1996 in Sapporo [2,24]. Our present results show that different genome types of HAdV-8 appeared in the three prevalence periods, which may indicate that a change in genome type resulted in the next prevalence period of HAdV-8. On the other hand, high frequency of infection in the population is regarded as a probable reason for the diverse evolution of HAdV-8 [7]. As HAdV-8 has become less common in Japan since 1997, a follow-up study of HAdV-8 should be completed in Japan and why we conducted this study.

HAdV-54 has recently been the major cause of EKC in Japan. The strain has occasionally been identified as HAdV-8 due to its weak reaction to HAdV-8 antiserum. On the basis

of the nucleotide sequence identities and phylogenetic analysis, HAdV-54 was much closer to the HAdV-8 strains over the entire genome than other HAdVs [15].

Our results show that genetic changes in HAdV-8 occur chronologically. HAdV-8 displays considerable variability. Because continued investigations of these variants might be helpful for defining the evolutionary tendency and to predict future outbreaks of HAdV infection, further genetic, epidemiological, and clinical surveillance of HAdVs should be performed.

ACKNOWLEDGMENTS

This work was supported by Grants-in-Aid for Scientific Research (KAKENHI) from Japan Society for the Promotion of Science (JSPS).

REFERENCES

1. Aoki K, Kaneko H, Kitaichi N, Ohguchi T, Tagawa Y, Ohno S. Clinical features of adenoviral conjunctivitis at the early stage of infection. Jpn J Ophthalmol 2011; 55:11-5. [PMID: 21331686]
2. Aoki K, Tagawa Y. A twenty-one year surveillance of adenoviral conjunctivitis in Sapporo, Japan. Int Ophthalmol Clin 2002; 42:49-54. [PMID: 12189615]
3. Tanaka-Yokogui K, Itoh N, Usui N, Takeuchi S, Uchio E, Aoki K, Usui M, Ohno S. New genome type of adenovirus serotype 19 causing nosocomial infections of epidemic keratoconjunctivitis in Japan. J Med Virol 2001; 65:530-3. [PMID: 11596089]
4. Jawetz E, Kimura S, Nicholas AN, Thygeson P, Hanna L. new type of APC virus from epidemic keratoconjunctivitis. Science 1955; 122:1190-1. [PMID: 13274081]
5. Fujii SI, Nakazono N, Sawada H, Ishii K, Kato M, Aoki K, Ohtsuka H, Fujinaga K. Restriction endonuclease cleavage analysis of adenovirus type 8: two new subtypes from patients with epidemic keratoconjunctivitis in Sapporo, Japan. Jpn J Med Sci Biol 1983; 36:307-13. [PMID: 6328068]
6. Fujii S, Nakazono N, Ishii K, Lin CC, Sheu MM, Chen CW, Fujinaga K. Molecular epidemiology of adenovirus type 8 (Ad 8) in Taiwan: four subtypes recovered during the period of 1980–1981 from patients with epidemic keratoconjunctivitis. Jpn J Med Sci Biol 1984; 37:161-9. [PMID: 6098752]
7. Chang C, Sheu M, Chern C, Lin K, Huang W, Chen C. Epidemic keratoconjunctivitis caused by a new genotype of adenovirus type 8 (Ad8)-a chronological review of Ad8 in Southern Taiwan. Jpn J Ophthalmol 2001; 45:160-6. [PMID: 11313048]
8. Ishii K, Nakazono N, Fujinaga K, Fujii S, Kato M, Ohtsuka H, Aoki K, Chen CW, Lin CC, Sheu MM, Lin KH, Oum BS, Lee SH, Chun CH, Yoshii T, Yamazaki S. Comparative studies on aetiology and epidemiology of viral conjunctivitis in three countries of East Asia–Japan, Taiwan and South Korea. Int J Epidemiol 1987; 16:98-103. [PMID: 3032816]
9. Guo DF, Shinagawa M, Aoki K, Sawada H, Itakura S, Sato G. Genome typing of adenovirus strains isolated from conjunctivitis in Japan, Australia, and the Philippines. Microbiol Immunol 1988; 32:1107-18. [PMID: 2851695]
10. Adhikary AK, Numaga J, Kaburaki T, Kawashima H, Araie M, Ikeda Y, Ogino T, Suzuki E, Ushijima H, Mukoyama A, Matsuno S, Inada T, Okabe N. Genetic characterisation of adenovirus type 8 isolated in Hiroshima city over a 15 year period. J Clin Pathol 2003; 56:120-5. [PMID: 12560390]
11. Adrian T, Wolf U, Lauer HJ, Wigand R. Restriction site mapping of adenovirus type 8 genome types. Res Virol 1990; 141:611-24. [PMID: 2087599]
12. de Jong JC, Demazure M, Legrand-Quillien MC, Le Lay G, Colin J, Wermenbol AG, Verweij-Uyterwaal MW, van der Avoort HG, Chastel C. New developments in the molecular epidemiology of adenovirus 8 keratoconjunctivitis. J Med Virol 1992; 38:102-7. [PMID: 1334124]
13. Tanaka K, Itoh N, Saitoh-Inagawa W, Uchio E, Takeuchi S, Aoki K, Soriano E, Nishi M, Junior RB, Harsi CM, Tsuzuki-Wang L, Durigon EL, Stewien KE, Ohno S. Genetic characterization of adenovirus strains isolated from patients with acute conjunctivitis in the city of Sao Paulo, Brazil. J Med Virol 2000; 61:143-9. [PMID: 10745247]
14. Ishiko H, Shimada Y, Konno T, Hayashi A, Ohguchi T, Tagawa Y, Aoki K, Ohno S, Yamazaki S. Novel human adenovirus causing nosocomial epidemic keratoconjunctivitis. J Clin Microbiol 2008; 46:2002-8. [PMID: 18385435]
15. Kaneko H, Iida T, Ishiko H, Ohguchi T, Ariga T, Tagawa Y, Aoki K, Ohno S, Suzutani T. Analysis of the complete genome sequence of epidemic keratoconjunctivitis-related human adenovirus type 8, 19, 37 and a novel serotype. J Gen Virol 2009; 90:1471-6. [PMID: 19264666]
16. Aoki K, Ishiko H, Konno T, Shimada Y, Hayashi A, Kaneko H, Ohguchi T, Tagawa Y, Ohno S, Yamazaki S. Epidemic keratoconjunctivitis due to the novel hexon-chimeric-intermediate 22,37/H8 human adenovirus. J Clin Microbiol 2008; 46:3259-69. [PMID: 18701656]
17. Wadell G, de Jong JC. Restriction endonucleases in identification of a genome type of adenovirus 19 associated with keratoconjunctivitis. Infect Immun 1980; 27:292-6. [PMID: 6247272]
18. Miura-Ochiai R, Shimada Y, Konno T, Yamazaki S, Aoki K, Ohno S, Suzuki E, Ishiko H. Quantitative detection and rapid identification of human adenoviruses. J Clin Microbiol 2007; 45:958-67. [PMID: 17229856]
19. Kimura M. A simple method for estimating evolutionary rates of base substitutions through comparative studies of nucleotide sequences. J Mol Evol 1980; 16:111-20. [PMID: 7463489]
20. Saitou N, Nei M. The neighbor-joining method: a new method for reconstructing phylogenetic trees. Mol Biol Evol 1987; 4:406-25. [PMID: 3447015]
21. Kaneko H, Suzutani T, Aoki K, Kitaichi N, Ishida S, Ishiko H, Ohashi T, Okamoto S, Nakagawa H, Hinokuma R, Asato Y, Oniki S, Hashimoto T, Iida T, Ohno S. Epidemiological and virological features of epidemic keratoconjunctivitis due to new human adenovirus type 54 in Japan. Br J Ophthalmol 2011; 95:32-6. [PMID: 20530657]
22. Tabbara KF, Omar N, Hammouda E, Akanuma M, Ohguchi T, Ariga T, Tagawa Y, Kitaichi N, Ishida S, Aoki K, Ishiko H, Ohno S. Molecular epidemiology of adenoviral keratoconjunctivitis in Saudi Arabia. Mol Vis 2010; 16:2132-6. [PMID: 21139691]

23. Adhikary AK, Banik U, Okabe N, Fujimoto T. Molecular characterization of human adenovirus type 8 (HAdV-8), including a novel genome type detected in Japan. Jpn J Infect Dis 2011; 64:493-8. [PMID: 22116328]
24. Saitoh-Inagawa W, Aoki K, Uchio E, Itoh N, Ohno S. Ten years' surveillance of viral conjunctivitis in Sapporo, Japan. Graefes Arch Clin Exp Ophthalmol 1999; 237:35-8. [PMID: 9951639]
25. de Jong TA, Wermenbol AG, van der Avoort HG, Wigand R. Genome type analysis of adenovirus 37 isolates. J Med Virol 1988; 25:77-83. [PMID: 2842449]

Articles are provided courtesy of Emory University and the Zhongshan Ophthalmic Center, Sun Yat-sen University, P.R. China. The print version of this article was created on 30 November 2011. This reflects all typographical corrections and errata to the article through that date. Details of any changes may be found in the online version of the article.

Graefes Arch Clin Exp Ophthalmol (2012) 250:239–245
DOI 10.1007/s00417-011-1843-1

BASIC SCIENCE

Astaxanthin increases choroidal blood flow velocity

Michiyuki Saito · Kazuhiko Yoshida · Wataru Saito · Akio Fujiya · Kazuhiro Ohgami · Nobuyoshi Kitaichi · Hiroki Tsukahara · Susumu Ishida · Shigeaki Ohno

Received: 4 January 2011 / Revised: 7 August 2011 / Accepted: 3 October 2011 / Published online: 10 November 2011

Abstract
Purpose Previous studies have reported that astaxanthin (AXT) has antioxidative and anti-inflammatory effects in addition to its ability to shorten blood transit times. As laser speckle flowgraphy (LSFG) can noninvasively visualize the hemodynamics of the choroidal circulation, we used the technique to evaluate whether continuous ingestion of 12 mg of AXT per day could increase quantitative blood flow velocity.
Methods In this randomized, double-blind, placebo-controlled study, we examined 20 healthy volunteers who ingested 12 mg AXT or placebo capsules over a 4-week period. LSFG was measured in the right eyes of all subjects at pre-ingestion, and at 2 and 4 weeks after the treatment of AXT. LSFG values were used to calculate the square blur rate (SBR), which is a quantitative index of relative blood flow velocity.
Results A significant increase of the macular SBR was seen 4 weeks after AXT ingestion when compared to the pre-ingestion values (Wilcoxon signed-rank test, $P=0.018$). In contrast, no statistical difference in the macular SBR was detected in the placebo group (Friedman test, $P=0.598$). No subjective or objective adverse events were found after the 12-mg AXT ingestion.
Conclusions Results suggest that administration of AXT over a 4-week period can elevate the choroidal blood flow velocity without any adverse effects.

Keywords Astaxanthin · Laser speckle flowgraphy · Choroidal blood flow velocity

This research project is registered with UMIN-CTR under the clinical trial registration number UMIN000004754.

M. Saito · K. Yoshida (✉) · W. Saito · A. Fujiya · K. Ohgami · N. Kitaichi · S. Ishida
Department of Ophthalmology,
Hokkaido University Graduate School of Medicine,
Nishi-7-chome, Kita 15-jou, Kita-ku,
Sapporo 060-8638, Japan
e-mail: kyoshida@med.hokudai.ac.jp

N. Kitaichi
Department of Ophthalmology,
Health Sciences University of Hokkaido,
Sapporo, Japan

H. Tsukahara
Fuji Chemical Industry Co., Ltd,
Tokyo, Japan

S. Ohno
Department of Ocular Inflammation and Immunology,
Hokkaido University Graduate School of Medicine,
Sapporo, Japan

Introduction

Astaxanthin (AXT) is one of the most common carotenoids, and is found in the red pigment of crustacean shells (e.g., crabs and shrimp), salmon, salmon roe, and members of Asteroidea (e.g., starfish). The chemical structure of this carotenoid has been shown to be modified, with the long-chain conjugate double bond and the b-ionone ring at both ends replaced by a keto- and hydroxyl-group respectively. Discovery of AXT's strong antioxidant effect has led to a large number of studies focusing on the compound, with these studies demonstrating a wide variety of biological activities that have included antioxidant [1], anti-tumor [2], anti-Helicobacter pylori effects [3], anti-arteriosclerosis [4], anti-inflammatory [5], or even perhaps control diabetic nephropathy (kidney disease) [6, 7].

Additionally, it has been reported that AXT ingestion has the effect of improving the microcirculation [8, 9]. A

microchannel array flow analyzer apparatus has shown, in vivo, that there is improvement of the blood rheology after ingestion of AXT 6 mg/day for 10 days in normal human subjects [8]. Moreover, Hussein G et al. reported a modulatory effect on nitric oxide (NO)-induced vasorelaxation by the NO-donor sodium nitroprusside ($P<0.05$) and hemorheological effect by decreasing the microchannel transit time of whole blood in spontaneously hypertensive rats with 7–9 weeks AXT administration [9].

Laser speckle flowgraphy (LSFG), which uses no contrast agents, has recently been used to investigate ocular blood flow distribution. LSFG is able to target moving red blood cells in the eye by using a diode laser (wavelength 830 nm) to illuminate the ocular fundus. The light that is reflected from the ocular tissue produces a speckled pattern on the plane where the area sensor is focused. The reflected lights from the moving erythrocytes then induce blurring within the speckle pattern. Square blur rate (SBR) is a quantitative index of the relative blood flow velocity that is calculated from variations in the blurring. It has been reported that after induction of branch retinal artery occlusion in monkey eyes, there is little change in the post-induction panoramic map when compared to vascular patterns prior to the occlusion. Therefore, as the blood flow velocities calculated by LSFG are believed to be choroidal in origin, they may be useful in evaluating the relative choroidal hemodynamics. We have previously reported that LSFG showed an increase in the foveolar choroidal blood velocity during the treatment of Vogt–Koyanagi–Harada (VKH) disease [10].

Recently, it has been elucidated that disturbance of choroidal circulation is involved in the pathogenesis of ocular diseases such as age-related macular degeneration (AMD) [11] and VKH [10]. Taken together, these reports suggest that treatment regimens designed to elevate the choroidal blood flow velocity should be of benefit in patients with these diseases. However, no investigations of AXT's effect on the choroidal circulation have ever been reported.

In the present study, we investigated the impact of oral administration of AXT on the effect to the choroidal blood circulation.

Materials and methods

Subjects

A total of 20 healthy volunteers (15 women, five men) were enrolled in the study.

This clinical trial was performed from January 2008 to February 2008 at Hokkaido University Hospital. Subjects were excluded from the study if any systemic or ocular abnormalities, such as diabetes or drug allergies, were found. In the case of female subjects, we also excluded pregnant subjects. Some of the volunteers did have mild or moderate refractive errors. This study followed the rules and guidelines of the Declaration of Helsinki, with all subjects signing an informed consent form after the nature and possible consequences of the study had been explained.

Study design

To collect the data, we used a randomized, double-blind, placebo-controlled design without crossover. Subjects were divided into two groups. The AXT group contained two men and eight women, and the placebo group three men and seven women. Over a duration of 4 weeks, the intervention group received two capsules of 6 mg AXT (total 12 mg) capsules once daily at 7 A.M., while the control group received identical-looking placebo capsules.

AXT

In this study, a soft gel capsule containing Haematococcus pluvialis natural AX of 6 mg was used (AX 5% by weight, Astarile® oil 50 F,Fuji Chemical Industry). In the previous report, the half-life of 9 mg ingestion was determined as 26.0±4.8 h [12]. For control groups, an identical-looking similar soft gel capsule containing no AXT was used.

Medical examinations

Prior to administration of the capsules, all subjects passed a screening examination, serologic test, and physical or medical examination. On the first day, 2 and 4 weeks after starting capsule ingestion, study physicians also examined each of the subjects for the presence of adverse events during subjects' visits. The information about adverse events was recorded daily, and collected at the time of subjects' visits. In addition, the serologic tests were performed at pre-ingestion and at 4 weeks after starting capsule ingestion.

LSFG

The LSFG were performed at pre-ingestion and then at 2 and 4 weeks after initiation of the ingestion. The measurements were performed in the morning about 4 hours after the capsule ingestion each time. The test was performed as reported elsewhere [13, 14]. Tropicamide 0.5% and phenylephrine hydrochloride 0.5% were used for mydoriatics. It has been shown that LSFG has little effect on the blood flow decrease at 30 minutes after the instillation of them [15].

Using a previously reported method, we were able to track the movement of the subject's eye in all directions during the measurement period [16]. To obtain these measurements, the patients had to maintain a good fixation for three cardiac cycles, which was approximately 7 seconds. The average of

five results was used as the SBR value. To evaluate changes in the relative blood flow velocity, a square was set at the macula (Fig. 1). An area of 600×280 pixels was created, so that the viewing angle was about 20 deg and included the macula. The average SBR was calculated by using the macular squares in the right eye.

To calculate the coefficient of the reproducibility of measurements, in our preliminary study, SBR was measured in 34 eyes of 34 healthy volunteers twice a day, with 1-minute intervals between each of the measurements. The equation used for the coefficient of the reproducibility of measurements was as follows:

$$|SBR1 - SBR2|/(1/2)(SBR1 + SBR2)(\%).$$

The coefficient of reproducibility for the SBR measurements for the 1-minute intervals was 2.1±0.4% (mean ± SEM, n=34).

Hemodynamics, IOP and OPP

Previous studies have demonstrated that there is a linear relationship between the choroidal blood flow and the ocular perfusion pressure (OPP) within a certain range [17]. After the LSFG measurements, the patient's blood pressure, pulse rate (PR) and intraocular pressure (IOP) were measured. Mean arterial pressure (MAP) was calculated from the systolic blood pressure (SBP) and the diastolic blood pressure (DBP), which was based on the following equation:

$$MAP = DBP + 1/3(SBP - DBP).$$

OPP was calculated using the following equation:

$$OPP = 2/3MAP - IOP.$$

Statistics

Comparisons between the changing rates for SBR and those seen at pretreatment were performed using a previously described statistical method [18]. Nonparametric tests such as the Friedman test or the Wilcoxon signed-rank test were used to analyze SBR values. Wilcoxon tests were performed to determine differences between periods for 3 times (pre-treatment vs 2 weeks, pre-treatment vs 4 weeks, 2 weeks vs 4 weeks) when time was a significant factor in the Friedman test. Wilcoxon tests were adjusted for multiplicity with the Bonferroni method.

The IOP, MAP, OPP and PR before, and 2 and 4 weeks after the treatments in the right eyes were compared using a repeated analysis of variance (ANOVA) test and a paired t-test. Since all of their values were found to have approximately normal distributions, we used the ANOVA and paired t-tests to analyze all of our data [19]. Differences were considered statistically significant when $P<0.05$.

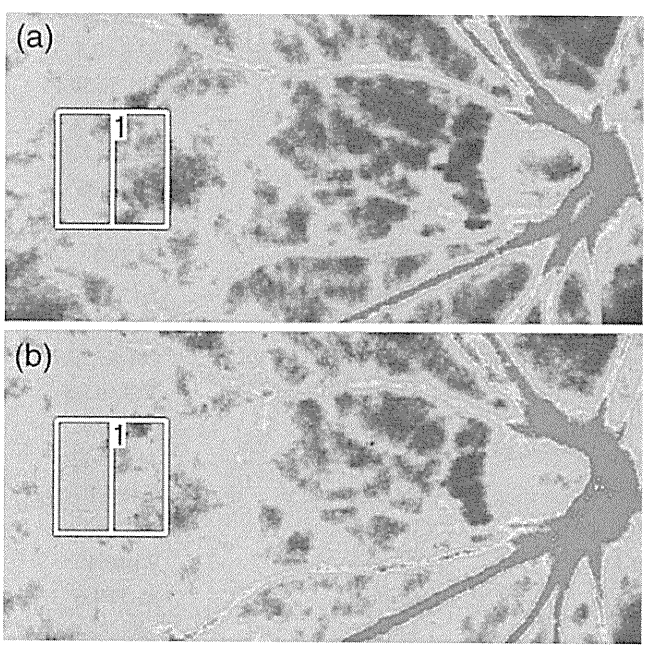

Fig. 1 Composite color map using the square blur rate (SBR) as measured by laser speckle flowgraphy (LSFG) at (**a**) the pretreatment and (**b**) 4 weeks after systemic 12 mg AXT treatment in the right eye. The *red color* indicates high SBR and the *blue color* indicates low SBR. The SBR increased at the macula during the 4-week treatment (square 1)

Results

Systemic data

Table 1 presents the subjects' backgrounds. At the start of the ingestion period, the mean age of the subjects was 38.2±11.7 and 38.8±6.8 (mean ± SD) years in the AXT and placebo

Table 1 Subjects' backgrounds. The mean age of the subjects at the start of the ingestion was 38.2±11.7 and 38.8±6.8 years in the AXT and placebo ingestion groups respectively. Body weight, body fat percentage and pulse rate were all within normal ranges, and did not differ significantly between the two groups (t-test, $P>0.1$, for all). All of the subjects in the AXT and the placebo ingestion groups had nearly identical backgrounds

	Placebo group	AXT group
Number of subjects	10	10
Age (years)	38.8±6.8	38.2±11.7
Weight (kg)	53.4±6.6	55.3±7.2
Body fat percentage (%)	25.5±3.6	24.3±5.4
Pulse rate (/min)	84.7±9.5	81.5±24.6

Mean value ± standard deviation

groups respectively. Body weight, body fat percentage, pulse rate, and all other measures were within normal ranges. There were no significant differences noted for the physical parameters between these groups ($P>0.05$, for all). The members of the AXT and placebo ingestion groups had nearly identical backgrounds.

Serologic test data

Serologic test data is summarized in Table 2. No significant differences were noted for the standard laboratory parameters between these two groups prior to capsule ingestion.

Furthermore, at 4 weeks after starting capsule ingestion, there were no significant differences between the two groups for the following parameters: white blood cells, red blood cells, hemoglobin, hematocrit, platelets, total protein, albumin, albumin–globulin ratio, glutamic oxaloacetic transaminase, glutamic pyruvic transaminase, lactate dehydrogenase, alkaline phosphatase, gamma-glutamyl transpeptidase, total bilirubin, creatinine, blood urea nitrogen, uric acid, creatine phosphokinase, total cholesterol, high-density lipoprotein cholesterol, triglyceride, sodium, potassium, chlorine, calcium, blood glucose levels, and hemoglobin A1c ($P>0.05$, for all).

Table 2 Serologic test data. The serologic tests were performed at pre-ingestion and at 4 weeks after starting capsule ingestion in both groups. At 4 weeks after starting capsule ingestion, there were no significant differences between the two groups for parameters listed in this table ($P>0.05$, for all). Moreover there were no significant changes for 4 weeks in either group ($P>0.05$, for all)

		Placebo group		AXT group	
Item	Unit	Before ingestion	4-week ingestion	Before ingestion	4-week ingestion
WBC	/μl	5998±2162.2	5931±1778.2	5089±803.3	5261±1857.4
RBC	$\times10^4$/μml	446.3±44.2	454.6±36	456.9±57.1	462.5±63.4
Hb	g/dl	14.1±1.3	13.9±1.2	14±1.3	13.7±1.6
Ht	%	41.6±3.6	43.2±3.3	42.4±4.3	43.5±4.7
MCV	fl	93.6±3.3	95.1±3.3	93.1±3	94.4±2.9
Plt	$\times10^4$/μml	25.3±6	24.5±6.6	21.8±3.6	22.6±3.1
TP	g/dl	7.3±0.2	7.3±0.3	7.2±0.3	7.2±0.6
Alb	g/dl	4.5±0.2	4.5±0.2	4.4±0.2	4.3±0.3
A/G	–	1.6±0.2	1.6±0.1	1.6±0.1	1.5±0.2
GOT	U/L	18.4±2.7	17.8±3	18.9±4	22±11.2
GPT	U/L	14.5±3	14±2.7	14.8±5.6	17.8±9.3
LDH	U/L	170.9±22.4	173.1±26.1	175.9±37.4	181.8±30.9
ALP	IU/l	161.9±35.3	153.8±34.7	165.6±46	161.9±52
γ-GTP	IU/l	19±5.1	18.2±5.2	24.2±19.9	22.2±12.2
T-Bil	mg/dl	0.7±0.1	0.8±0.1	0.7±0.2	0.8±0.3
Cre	mg/dl	0.6±0	0.6±0	0.6±0.1	0.6±0.1
BUN	mg/dl	12±2.8	12.1±2.3	15.4±3.3	14.3±4
UA	mg/dl	4.7±1.1	4.5±0.9	4.7±1.6	4.7±1.6
CPK	IU/l	85.5±33.3	90.6±36.6	88.7±27.6	97.3±36.8
TC	mg/dl	194.7±24.1	192.3±24.5	190.1±32.9	181.8±30.7
HDL	mg/dl	74.7±17.7	76.8±16.8	72±17.4	72.1±13.5
TG	mg/dl	81.1±48.9	63.3±30.3	56±21.6	47.5±17
Na	mEq/L	141.2±1.5	141.5±1.1	140.8±1.5	141.1±2.2
K	mEq/L	4.2±0.5	4.2±0.7	4.5±0.6	4.4±1.1
Cl	mEq/L	102.8±1.9	103.4±0.6	103.2±2	103.3±2.6
Ca	mEq/L	9±0.3	9.2±0.3	8.9±0.3	9.1±0.4
FBS	mg/dl	83.8±6.4	87.3±4.9	88±6.6	85.8±4.6
A1c	%	4.5±0.4	4.5±0.3	4.7±0.2	4.8±0.2

WBC = white blood cells; RBC = red blood cells; Hb = hemoglobin; Ht = hematocrit; MCV = mean cell hemoglobin concentration; Pt = platelets; TP = total protein; Alb = albumin; A/G = albumin–globulin ratio; GOT = glutamic oxaloacetic transaminase; GPT = glutamic pyruvic transaminase; LDH = lactate dehydrogenase; ALP = alkaline phosphatase; γ-GTP = gamma–glutamyl transpeptidase; T-Bil = total bilirubin; creatinine; Cre = creatine phosphokinase; BUN = blood urea nitrogen; UA = uric acid; CPK = creatine phosphokinase; TC = total cholesterol; HDL = high-density lipoprotein cholesterol; TG = triglyceride; Na = sodium; K = potassium; Cl = chlorine; Ca = calcium; FBS = fasting blood sugar levels; A1c = hemoglobin A1c ; mean ± standard deviation

Refractive errors and BCVA

Pre-treatment average spherical equivalent of the refractive errors in the right eye were −1.15 (ranging from 2.63 to −4.25) diopters in the AXT group and −1.28 (from 2.75 to −4.0) diopters in the placebo group. There was no significant difference in the refractive errors noted between the groups (P=0.89, t-test).

The mean log MAR best-corrected visual acuity (BCVA) values for the right eyes that were obtained prior to and at 4 weeks after beginning of capsule ingestion were 0.106 and 0.144 in the placebo group and 0.018 and 0.104 in the AXT group respectively. There were no significant differences in either group (placebo group P=0.863, AXT group P=0.571, paired t-test).

Hemodynamics, OPP and IOP

As seen in Table 3, no significant differences were noted for the MAP (t-test, P=0.99), IOP (t-test, P=0.16), OPP (t-test, P=0.52), and PR (t-test, P=0.71) between the groups prior to capsule ingestion. In the AXT group, there were also no significant differences for the IOP of the right eyes (repeated ANOVA, P=0.14), MAP (repeated ANOVA, P=0.59), and OPP (repeated ANOVA, P=0.28) for 4 weeks. The pulse rate was also measured at 2 and 4 weeks after start of treatment. There were no significant changes both in AXT and placebo groups (repeated ANOVA, P=0.45 and P=0.09 respectively).

Table 3 Variations in hemodynamic parameters observed during administration of AXT or the placebo. No significant differences were noted for the MAP (t-test, P=0.99), IOP (t-test, P=0.16), or OPP (t-test, P=0.52) between the groups prior to capsule ingestion. The placebo and AXT groups exhibited no significant differences for the MAP, IOP, and OPP between the pre-ingestion results and the results at 2 or 4 weeks after capsule ingestion (repeated ANOVA, P>0.1).The pulse rate was also measured at 2 and 4 weeks after start of treatment. There were no significant changes in either the AXT or the placebo group (repeated ANOVA, P=0.45 and P=0.09 respectively)

	Before ingestion	2-week ingestion	4-week ingestion
Placebo group			
MAP (mmHg)	89±2	87±2	85±2
IOP (mmHg)	15±0.8	15±0.6	14±0.7
OPP (mmHg)	45±1	43±1	42±2
PR (/min)	85±3	81±3	77±3
AXT group			
MAP (mmHg)	89±2	89±2	88±3
IOP (mmHg)	14±0.6	14±0.7	14±0.9
OPP (mmHg)	46±2	46±1	44±2
PR (/min)	82±8	74±3	74±3

MAP = mean arterial pressure; IOP = intraocular pressure; OPP = ocular perfusion pressure; PR = pulse rate; mean ± standard error (n=10)

LSFG data

With regard to the choroidal blood flow velocity, a summary of the measurement results for both groups' SBR at the macular area during capsule administration is shown in Fig. 2. Because SBR is a quantitative index of the "relative" blood flow velocity, the SBR at 2 and 4 weeks after AXT ingestion was indicated as ratio to the pre-ingestion values. Therefore, no error bars are shown in the pre-treatment levels of SBR as in the manuscripts previously reported [19, 20].

Significant changes in the SBR values at the macular area were noted after AXT ingestion (Friedman test, P=0.016). In addition, there were significant increases in the SBR at the macula at 4 weeks after AXT ingestion when compared to the

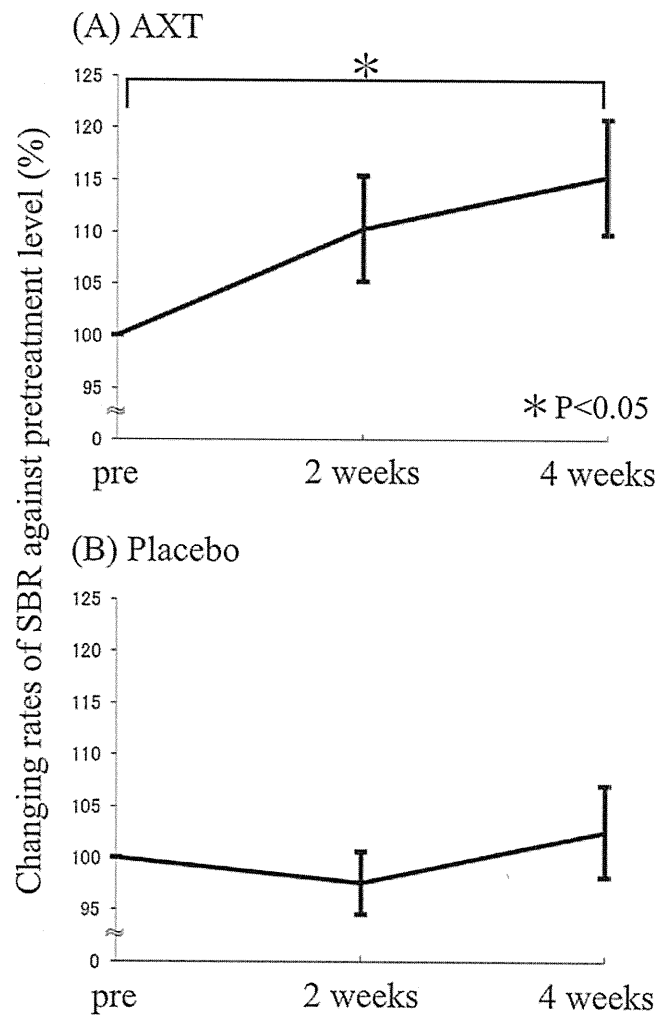

Fig. 2 Changing rates of macular flow compared to the pretreatment level (n=10; mean ± standard error) after the ingestion of astaxanthin (**a**) and placebo (**b**). Significant changes in the SBR values at the macular area were noted after AXT ingestion (Friedman test, P=0.016). The SBR at the macula significantly increased at 4 weeks after AXT ingestion as compared to pre-ingestion values (Wilcoxon signed-rank test, P=0.018). Conversely, there were no significant changes in the SBR in the placebo group (Friedman test, P=0.598)

pre-ingestion values (Wilcoxon signed-rank test, P=0.018). When the changing rates of the macular flow were compared to the pretreatment levels, a 10.3% increase was noted at 2 weeks, while a 15.3% increase was noted at 4 weeks after the AXT administration.

In contrast, no statistical differences in the macular SBR were detected among pre-, 2-week and 4-week ingestion values in the placebo group (Friedman test, P=0.598).

Adverse effects

There were no subjects in either group that exhibited adverse effects at any time during the study.

Discussion

In the present study, we used LSFG to evaluate macular area blood flow velocity prior to and after ingestion of AXT. It has been reported that the choroidal blood flow exceeds the retinal flow by approximately 96% in areas outside of the fovea [21]. In addition, there are no large retinal vessels found near the fovea [22]. Therefore, the SBR calculations we performed at the square of the macula can be considered to reflect the choroidal blood flow velocity.

The significant increase in the SBR was noted in volunteers who continuously ingested 12 mg of AXT per day over a 4-week period. In contrast, no statistical differences in the macular SBR were detected among pre-, 2-week and 4-week in the placebo group. Upon continuous ingestion of 12 mg of AXT, there were no abnormal findings or adverse events noted either subjectively or objectively, which included changes in the arterial blood pressure and heart rate response (Table 3).These results suggest that a 4-week AXT administration can elevate the choroidal blood flow velocity without adverse effects.

Our results showed that AXT increases the choroidal blood flow velocity. Since no significant differences were noted for the OPP prior to, and at 2 and 4 weeks after ingestion, the choroidal blood flow velocity increase was not due to systemic hemodynamic changes, but rather was due to either vasodilation in the choroid or changes in blood rheology. In this study, we were not discriminative about which mechanism was attributed to the increase of SBR. The vasodilation due to a modulatory effect on NO-induced vasorelaxation might also be responsible for even normal human chroidal vessels. On the other hand, it has been previously reported that AXT ingestion shortens the blood transit time [8, 9], suggesting that AXT improves the blood rheology. A similar hemorheological mechanism might also be responsible for the elevated choroidal blood flow velocities.

In the previous reports, the mechanism responsible for the improvement in blood rheology by AXT was not determined. However, it has been reported that AXT prevents over-oxidation of lipids via its strong antioxidant effect, and controls oxidation of low density lipoprotein [23]. AXT is believed to be able to effectively work against oxidation in lipid metabolism, and also has been shown to be widely distributed in the lipoprotein areas of the body [24, 25]. The actions of AXT are thought to work by preventing oxidation of the biomembranes, which includes the cell membranes. Hence, it was hypothesized that there was an antioxidant effect for both within and outside of the lipid double membrane of erythrocytes, which renders the form flexible, thereby making it possible to longitudinally obtain such suitable membranes [8].

This study is intended to be an exploratory proof of concept study, requiring confirmatory studies in the future. While this study has shown that AXT significantly increases the choroidal blood flow in the absence of any side-effects, it is still unknown as to whether this effect is temporary or permanent. With regard to the design of this study, the statistic was conducted with small sample size. However, in this study, when the two-sided significance level was 0.05, the powers of analysis of the Friedman test in the AXT group and the placebo group were 0.91 and 0.78 respectively. These values are almost sufficient, because most researchers assess the power of their tests using 0.80 as a standard for adequacy [26]. Additionally, the change of SBR was examined using a randomized, double-blind, placebo-controlled without cross-over design. The intra-group comparison for the changing rates of SBR by the Wilcoxon test clearly indicated the effect of AXT on the SBR. However, studies that examine these long-term effects on wider cohort are desirable for the future evaluation of the AXT effects on choroidal circulation in humans.

Acknowledgments This work was supported by the 21st Century COE Program "Topological Science and Technology", Ministry of Education, Culture, Sports, Science and Technology, Japan, and a grant from the Ministry of Education, Culture, Sports and Technology, Japan.

Conflict of interest Hiroki Tsukahara is an employee of Fuji Chemical Industry Co., Ltd. The AXT capsules were provided by the company.

References

1. Esterbauer H, Jurgens G, Quehenberger O, Koller E (1987) Autoxidation of human low density lipoprotein: loss of polyunsaturated fatty acids and vitamin E and generation of aldehydes. J Lipid Res 28:495–509
2. Tanaka T, Makita H, Ohnishi M, Mori H, Satoh K, Hara A (1995) Chemoprevention of rat oral carcinogenesis by naturally occurring xanthophylls, astaxanthin and canthaxanthin. Cancer Res 55:4059–4064

3. Wang X, Willen R, Wadstrom T (2000) Astaxanthin-rich algal meal and vitamin C inhibit Helicobacter pylori infection in BALB/cA mice. Antimicrob Agents Chemother 44:2452–2457
4. Li W, Hellsten A, Jacobsson LS, Blomqvist HM, Olsson AG, Yuan XM (2004) Alpha-tocopherol and astaxanthin decrease macrophage infiltration, apoptosis and vulnerability in atheroma of hyperlipidaemic rabbits. J Mol Cell Cardiol 37:969–978
5. Ohgami K, Shiratori K, Kotake S, Nishida T, Mizuki N, Yazawa K, Ohno S (2003) Effects of astaxanthin on lipopolysaccharide-induced inflammation in vitro and in vivo. Invest Ophthalmol Vis Sci 44:2694–2701
6. Uchiyama K, Naito Y, Hasegawa G, Nakamura N, Takahashi J, Yoshikawa T (2002) Astaxanthin protects beta-cells against glucose toxicity in diabetic db/db mice. Redox Rep 7:290–293
7. Naito Y, Uchiyama K, Aoi W, Hasegawa G, Nakamura N, Yoshida N, Maoka T, Takahashi J, Yoshikawa T (2004) Prevention of diabetic nephropathy by treatment with astaxanthin in diabetic db/db mice. Biofactors 20:49–59
8. Miyawaki H, Takahashi J, Tsukahara H, Takehara I (2008) Effects of astaxanthin on human blood rheology. J Clin Biochem Nutr 43:69–74
9. Hussein G, Nakamura M, Zhao Q, Iguchi T, Goto H, Sankawa U, Watanabe H (2005) Antihypertensive potential and mechanism of action of astaxanthin: II. Vascular reactivity and hemorheology in spontaneously hypertensive rats. Biol Pharm Bull 28:967–971
10. Hirose S, Saito W, Yoshida K, Saito M, Dong Z, Namba K, Satoh H, Ohno S (2008) Elevated choroidal blood flow velocity during systemic corticosteroid therapy in Vogt–Koyanagi–Harada disease. Acta Ophthalmol 86:902–907
11. Grunwald JE, Metelitsina TI, Dupont JC, Ying GS, Maguire MG (2005) Reduced foveolar choroidal blood flow in eyes with increasing AMD severity. Invest Ophthalmol Vis Sci 46:1033–1038
12. Ohi Y, Kitamura A, Tsukahara H, Takahashi J, Itakura H (2011) The supplementation inquest of astaxanthin on blood kinetics. Journal of Clinical Therapeutics & Medicines 27: [Epub ahead of print]
13. Tamaki Y, Araie M, Kawamoto E, Eguchi S, Fujii H (1995) Non-contact, two-dimensional measurement of tissue circulation in choroid and optic nerve head using laser speckle phenomenon. Exp Eye Res 60:373–383
14. Isono H, Kishi S, Kimura Y, Hagiwara N, Konishi N, Fujii H (2003) Observation of choroidal circulation using index of erythrocytic velocity. Arch Ophthalmol 121:225–231
15. Takayama J, Mayama C, Mishima A, Nagahara M, Tomidokoro A, Araie M (2009) Topical phenylephrine decreases blood velocity in the optic nerve head and increases resistive index in the retinal arteries. Eye Lond 23:827–834
16. Tamaki Y, Araie M, Kawamoto E, Eguchi S, Fujii H (1994) Noncontact, two-dimensional measurement of retinal microcirculation using laser speckle phenomenon. Invest Ophthalmol Vis Sci 35:3825–3834
17. Riva CE, Titze P, Hero M, Petrig BL (1997) Effect of acute decreases of perfusion pressure on choroidal blood flow in humans. Invest Ophthalmol Vis Sci 38:1752–1760
18. Sugiyama T, Utsumi T, Azuma I, Fujii H (1996) Measurement of optic nerve head circulation: comparison of laser speckle and hydrogen clearance methods. Jpn J Ophthalmol 40:339–343
19. Ishii K, Tomidokoro A, Nagahara M, Tamaki Y, Kanno M, Fukaya Y, Araie M (2001) Effects of topical latanoprost on optic nerve head circulation in rabbits, monkeys, and humans. Invest Ophthalmol Vis Sci 42:2957–2963
20. Hayashi N, Ikemura T, Someya N (2011) Effects of dynamic exercise and its intensity on ocular blood flow in humans. Eur J Appl Physiol 111:2601–2606
21. Alm A, Bill A (1973) Ocular and optic nerve blood flow at normal and increased intraocular pressures in monkeys (Macaca irus): a study with radioactively labelled microspheres including flow determinations in brain and some other tissues. Exp Eye Res 15:15–29
22. Schatz H (1994) Fluorescein angiography: basic principles and interpretation. In: Ryan SJ (ed) Retina. Mosby, St. Louis, pp 911–984
23. Iwamoto T, Hosoda K, Hirano R, Kurata H, Matsumoto A, Miki W, Kamiyama M, Itakura H, Yamamoto S, Kondo K (2000) Inhibition of low-density lipoprotein oxidation by astaxanthin. J Atheroscler Thromb 7:216–222
24. Osterlie M, Bjerkeng B, Liaaen-Jensen S (2000) Plasma appearance and distribution of astaxanthin E/Z and R/S isomers in plasma lipoproteins of men after single dose administration of astaxanthin. J Nutr Biochem 11:482–490
25. Coral-Hinostroza GN, Ytrestoyl T, Ruyter B, Bjerkeng B (2004) Plasma appearance of unesterified astaxanthin geometrical E/Z and optical R/S isomers in men given single doses of a mixture of optical 3 and 3'R/S isomers of astaxanthin fatty acyl diesters. Comp Biochem Physiol C Toxicol Pharmacol 139:99–110
26. Ellis PD (2010) The essential guide to effect sizes: statistical power, meta-analysis, and the interpretation of research results. Cambridge University Press, Cambridge UK

Journal of General Virology (2011), 92, 1251–1259 DOI 10.1099/vir.0.030361-0

Recombination analysis of intermediate human adenovirus type 53 in Japan by complete genome sequence

Hisatoshi Kaneko,[1] Koki Aoki,[2] Susumu Ishida,[2] Shigeaki Ohno,[3] Nobuyoshi Kitaichi,[3,4] Hiroaki Ishiko,[5] Tsuguto Fujimoto,[6] Yoshifumi Ikeda,[7] Masako Nakamura,[8] Gabriel Gonzalez,[9] Kanako O. Koyanagi,[9] Hidemi Watanabe[9] and Tatsuo Suzutani[1]

Correspondence
Hisatoshi Kaneko
h-kane@chive.ocn.ne.jp

[1]Department of Microbiology, Fukushima Medical University School of Medicine, Fukushima, Japan

[2]Department of Ophthalmology, Hokkaido University Graduate School of Medicine, Sapporo, Japan

[3]Department of Ocular Inflammation and Immunology, Hokkaido University Graduate School of Medicine, Sapporo, Japan

[4]Department of Ophthalmology, Health Sciences University of Hokkaido, Sapporo, Japan

[5]Host Defense Laboratory, Mitsubishi Chemical Medience Corporation, Tokyo, Japan

[6]National Institute of Infectious Diseases, Tokyo, Japan

[7]Hiroshima City Institute of Public Health, Hiroshima, Japan

[8]Fukui Prefectural Institute of Public Health and Environmental Science, Fukui, Japan

[9]Laboratory of Genome Sciences, Research Groups of Bioinformatics, Division of Bioengineering and Bioinformatics, Hokkaido University Graduate School of Information Science and Technology, Sapporo, Japan

Received 6 January 2011
Accepted 28 February 2011

Human adenovirus type 53 (HAdV-53) has commonly been detected in samples from epidemic keratoconjunctivitis (EKC) patients in Japan since 1996. HAdV-53 is an intermediate virus, containing hexon-chimeric, penton base and fiber structures similar to HAdV-22 and -37, HAdV-37 and HAdV-8, respectively. HAdV-53-like intermediate strains were first isolated from EKC samples in Japan in the 1980s. Here, the complete genome sequences of three such HAdV-53-like intermediate strains (870006C, 880249C and 890357C) and four HAdV-53 strains were determined, and their relationships were analysed. The seven HAdV strains were classified into three groups, 870006C/880249C, 890357C and the four HAdV-53 strains, on the basis of phylogenetic analyses of the partial and complete genome sequences. HAdV strains within the same group showed the highest nucleotide identities (99.87–100.00 %). Like HAdV-53, the hexon loop 1 and 2 regions of 870006C, 880249C and 890357C showed the highest identity with HAdV-22. However, these strains did not show a hexon-chimeric structure similar to HAdV-22 and -37, or a penton base similar to HAdV-37. The fiber genes of 870006C and 880249C were identical to that of HAdV-37, but not HAdV-8. Thus, the three intermediate HAdVs isolated in the 1980s were similar to each other but not to HAdV-53. The recombination breakpoints were inferred by the Recombination Detection Program (RDP) using whole-genome sequences of these seven HAdV and of 12 HAdV-D strains from GenBank. HAdV-53 may have evolved from intermediate HAdVs circulating in the 1980s, and from HAdV-8, -22 and -37, by recombination of sections cut at the putative breakpoints.

INTRODUCTION

Adenoviruses are non-enveloped, dsDNA viruses with icosahedral capsids (Swenson *et al.*, 2003). Human adenoviruses (HAdVs) belong to the genus *Mastadenovirus* of the family *Adenoviridae* and infect billions of people

The GenBank/EMBL/DDBJ accession numbers for the nucleotide sequences presented in this study are AB605240–AB605246.

worldwide, causing various diseases, including conjunctivitis, respiratory disease, gastroenteritis in infants and young children, and haemorrhagic cystitis (Wold & Horwitz, 2007). To date, 51 types have been identified and classified into six species, HAdV-A to -F, on the basis of nucleotide and deduced amino acid sequences (Benko *et al.*, 2005). Recently, new HAdV types were proposed on the basis of the analysis of complete genome sequences (Jones *et al.*, 2007; Ishiko *et al.*, 2008; Ishiko & Aoki, 2009; Walsh *et al.*, 2009, 2010). Conjunctivitis due to HAdV is caused mainly by HAdV-3 (species HAdV-B), -4 (HAdV-E) and -8, -19, -37, -53 and -54 (HAdV-D) (Aoki & Tagawa, 2002; Tabbara *et al.*, 2010; Kaneko *et al.*, 2011a). Among these, the five HAdV-D strains are known to cause epidemic keratoconjunctivitis (EKC) with severe symptoms, such as severe discharge, lachrymation, pseudomembrane formation and multiple subepithelial corneal infiltrates (Aoki & Tagawa, 2002; Aoki *et al.*, 2011).

HAdV-53 is an intermediate virus formed by recombination among different HAdV types. The hexon gene in HAdV-53 shows a chimeric structure, and the loop region, which contains the neutralization epitope, and the 3′-conserved region 4 (C4) show the highest nucleotide identity with HAdV-22 and -37, respectively. HAdV-53 is also neutralized by HAdV-22 antisera (Walsh *et al.*, 2009; Aoki *et al.*, 2011). In contrast, the penton base and fiber genes in HAdV-53 show the highest identity with HAdV-37 and -8, respectively. HAdV types are traditionally numbered by neutralization test (NT). However, according to analysis of the complete genome sequences, HAdV-53 is identical to HAdV-22 in only the hexon loop regions, with other regions differing in sequence from those of HAdV-22. HAdV-53 was therefore numbered as a new HAdV type on the basis of recombination and bioinformatics analyses of the complete genome sequence. To date, HAdV-53 has only been isolated from EKC patients in Japan and Germany (Engelmann *et al.*, 2006; Aoki *et al.*, 2008; Walsh *et al.*, 2009). In Japan, HAdV-53 was reported in samples from EKC patients in different cities between 2003 and 2004 (Aoki *et al.*, 2008). We redetermined the HAdV type in a number of conjunctival samples obtained from EKC patients before 2000 in Japan (Kaneko *et al.*, 2011a). Our results showed that HAdV-53 had already been isolated from EKC patients in 1996, although most HAdV-53 isolates were mistyped as other HAdV types, such as HAdV-8, -22 or -37, on the basis of NT or molecular analysis of the partial genome. HAdV-53 has been isolated in a number of cities since 1996 and has recently become the third most commonly detected strain in EKC patients in Japan behind HAdV-37 and -54 (Aoki *et al.*, 2008; Kaneko *et al.*, 2011a).

A remarkable characteristic of HAdV-53 is that only the loop region of the hexon gene shows identity to HAdV-22, which rarely causes EKC. In the 1980s, two intermediate recombinant HAdVs were isolated from EKC patients in Hiroshima, in the western part of Japan, and reported as HAdV-22/H10,19,37 and -22/H8,9 on the basis of an NT and haemagglutination inhibition (HI) test (Noda *et al.*, 1991). These isolates were neutralized by HAdV-22 antisera and, as with HAdV-53, contained regions similar to those of HAdV-8 or -37 in the genome. Thus, these intermediate HAdVs isolated in the 1980s were similar to HAdV-53.

In this study, we determined the complete genome sequences of three HAdV-53-like intermediate HAdVs isolated in the 1980s and four HAdV-53 strains currently in circulation in Japan. Through recombination-event searches and bioinformatics analyses using complete genome sequences, the genomic relationships among these HAdVs were evaluated.

RESULTS

General properties and organization of the complete genome of the seven intermediate HAdV strains

The genome size and G+C content of the seven HAdV strains are shown in Table 1. The genome size and percentage G+C content were found to be almost identical among the seven strains. The genome organization of the seven strains was determined by analysis of the ORFs and alignment of their nucleotide sequences. The layout of the early and late regions in the complete sequences of these strains is shown in Fig. 1(a). The number of genes and their genome organization for each of the seven strains were identical to those of recently determined HAdV-D sequences (Robinson *et al.*, 2008; Kaneko *et al.*, 2009, 2011b; Walsh *et al.*, 2009), although the size of some ORFs varied slightly between strains or types (data not shown).

Phylogenetic analysis of identities among the complete nucleotide sequences of the seven intermediate HAdV and the other HAdV-D strains

Phylogenetic analyses of the complete genome sequences were carried out using the seven HAdVs described above and 12 fully sequenced HAdV-D strains from GenBank. The seven recombinant HAdVs in this study formed a single cluster and did not form a cluster with any other HAdV-D type (Fig. 2a). Three subclusters were formed within the single cluster. The 870006C and 880249C strains showed the highest identity (99.89 %) and formed a single subcluster. Similarly, the four HAdV-53 strains also showed the highest identities (99.87–100.00 %) with each other and formed a second subcluster. The 890357C strain alone formed a separate subcluster. Thus, the seven strains were classified into three groups containing 870006C/880249C, 890357C and the four HAdV-53 strains, respectively. The nucleotide identities among HAdV strains in the different groups were 96.99–98.55 %. The identities of the complete genome sequences among the seven recombinant HAdVs and other HAdV-D strains were even lower at 91.63–94.79 %.

Table 1. Genome size, G+C content and HAdV type in five regions of the seven intermediate HAdVs

ND, Not detected.

Strain/place/year	Genome size	G+C content (mol%)	HAdV type detected by phylogenetic analysis				
			Penton base	Loops 1 and 2 in hexon	C4 in hexon	E3	Fiber
870006C/Hiroshima/1987	35048	56.76	ND	HAdV-22	ND	ND	HAdV-37
880249C/Hiroshima/1988	35045	56.75	ND	HAdV-22	ND	ND	HAdV-37
890357C/Hiroshima/1989	35118	56.44	ND	HAdV-22	ND	ND	HAdV-8
960528C/Hiroshima/1996 (HAdV-53)	35137	56.39	HAdV-37	HAdV-22	HAdV-37	ND	HAdV-8
C075/Matsuyama/2003 (HAdV-53)	35137	56.37	HAdV-37	HAdV-22	HAdV-37	ND	HAdV-8
FS161/Fukui/2004 (HAdV-53)	35116	56.76	HAdV-37	HAdV-22	HAdV-37	ND	HAdV-8
FS165/Fukui/2004 (HAdV-53)	35116	56.76	HAdV-37	HAdV-22	HAdV-37	ND	HAdV-8

Phylogenetic analysis of the hexon, penton base, fiber gene and E3 region sequences

The HAdV genome contains four highly variable regions, the hexon, penton base and fiber genes and the E3 region (Kaneko *et al.*, 2009). Phylogenetic analyses of these regions were carried out using the seven HAdV strains in this study as well as other HAdV-D types. The entire hexon, penton base and fiber gene and the E3 region sequences of 32, 14, 15 and 13 HAdV-D types, respectively, were obtained from GenBank and used for the analyses. In the hexon gene, phylogenetic analyses of loops 1 and 2 and C4 were carried out.

Phylogenetic analysis of loops 1 and 2 in the hexon gene showed that all seven HAdV strains, including HAdV-53, in this study formed a cluster with HAdV-22 (Fig. 2b, c). In contrast, phylogenetic analysis of C4 in the hexon gene (Madisch *et al.*, 2005) revealed that the four HAdV-53 strains formed a monophyletic cluster with HAdV-37, whereas the other three strains did not form a monophyletic cluster with any HAdV-D strain (Fig. 2d). Thus, the three recombinant viruses isolated in the 1980s, 870006C, 880249C and 890357C, did not show a hexon-chimeric structure of HAdV-22 and -37.

Phylogenetic analysis of the penton base gene revealed that the four HAdV-53 strains formed a monophyletic cluster with HAdV-37, whereas the other three strains did not form a monophyletic cluster with any HAdV-D strain (Fig. 2e). Phylogenetic analysis of the E3 region revealed that all seven strains formed a single cluster but did not form a monophyletic cluster with any other HAdV-D strain (Fig. 2f). Phylogenetic analysis of the fiber gene showed that all four HAdV-53 strains, as well as 890357C, formed a cluster with HAdV-8, and that the other two HAdV strains, 870006C and 880249C, formed a cluster with HAdV-37 (Fig. 2g). The HAdV type of each region in the seven recombinant HAdV strains is summarized in Table 1.

Similarity plot analysis of the complete genome sequences of HAdV-8, -22 and -37 and the seven intermediate HAdV strains

Similarity plots were performed on the seven HAdV strains in this study, which were classified into three groups (870006C/880249C, 890357C and HAdV-53 strains) by phylogenetic analysis of complete genome sequence (Fig. 2a). The identities among strains within the same groups were high, with little variability over the entire genome (Fig. 1c). Identity over the entire genome among the 870006C and 890357C strains was examined and found to be low in late region 5 (L5) and E4, with that of the fiber gene in L5 being particularly low (Fig. 1d). Similarly, identity among the 870006C and HAdV-53 strains was also low in L5 and E4. In addition, the identities for the sequence located between the pTP gene in E2B and the 100 kDa protein in L4, except for the hexon loop region, among these strains were a little lower than those of 870006C and 890357C. In contrast, the identities of E1A and E1B among the 870006C and HAdV-53 strains were higher than those of 870006C and 890357C (Fig. 1e). The identities among 890357C and the HAdV-53 strains were shown to be lower for the sequence located between the pTP gene in E2B and the 100 kDa protein in L4, except for the hexon loop region, as shown among the 870006C and HAdV-53 strains. The identities of the other regions over the entire genome, including L5 and E4, were high (Fig. 1f).

Similarity plot analyses of HAdV-8, -22 and -37 and the seven intermediate HAdV strains were also carried out (Fig. 1g–i). HAdV-8 showed a high identity in L5 and E4 with the 890357C and HAdV-53 strains, and HAdV-22 showed a high identity for just the loop region in the hexon gene of all seven HAdVs. The regions with a high identity for HAdV-37 were E1A and E1B in the 870006C and 880249C strains, L5 and E4 in the 890357C strains, and the sequence located between the pTP gene in E2B and the 100kDa protein in L4, excluding the hexon loop region, in HAdV-53.

Phylogenetic analysis of sections cut at the putative recombination breakpoints

We inferred the recombination regions by comparing the whole genomes of the seven HAdV strains in this study and 12 fully sequenced HAdV-D strains (HAdV-8, -9, 17, -19, -22, -26, -28, -37, -46, -48, -49 and -54) from GenBank

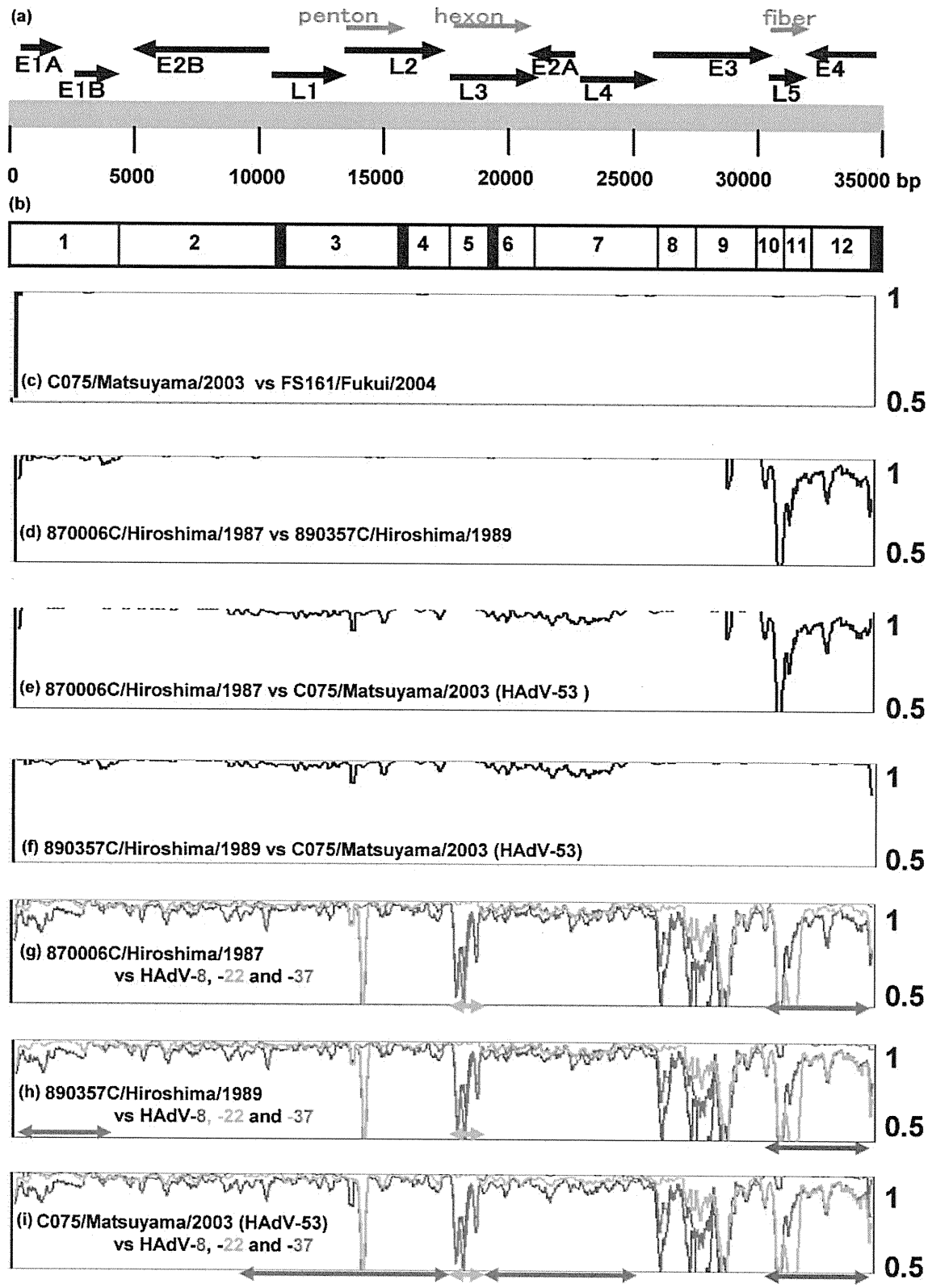

Fig. 1. Genome organization of the seven complete HAdV genomes. (a) The grey horizontal bar in the centre shows the linear double-stranded HAdV genome with each vertical line representing 5000 bp. Transcription units are shown by black arrows relative to their position and orientation in the HAdV genome. Grey arrows show the positions of the penton, hexon and fiber genes. (b) Twelve sections cut at the putative recombinant breakpoints. The solid areas indicate short sections of <1000 bp in length that were excluded from the analyses. (c–i) Similarity plots of the complete genome sequence between C075/

Matsuyama/2003 (HAdV-53) and FS161/Fukui/2004 (HAdV-53) (c), 870006C/Hiroshima/1987 and 890357C/Hiroshima/1989 (d), 870006C/Hiroshima/1987 and C075/Matsuyama/2003 (HAdV-53) (e), 890357C/Hiroshima/1989 and C075/Matsuyama/2003 (HAdV-53) (f), 870006C/Hiroshima/1987 and HAdV-8, -22 and -37 (g), 890357C/Hiroshima/1989 and HAdV-8, -22 and -37 (h), and C075/Matsuyama/2003 (HAdV-53) and HAdV-8, -22 and -37 (i), generated using SimPlot 3.5.1. The vertical axis indicates the nucleotide identity, expressed as a decimal. The horizontal axis indicates the nucleotide position of the complete sequences. HAdV-8, -22 and -37 are shown as blue, green and red lines, respectively, in (g), (h) and (i). Double-headed arrows in (g), (h) and (i) show the regions with the highest nucleotide identity with HAdV-8 (red), -22 (green) and -37 (blue).

using RDP (Martin *et al.*, 2005b). As a result, 15 putative recombination breakpoints were identified, thereby cutting the HAdV genomes into 16 sections. Among these sections, four shorter sections of <1000 bp were excluded from the analyses. Phylogenetic analyses were performed on the 12 sections that were >1000 bp in length (Fig. 1b), and the type among the 12 HAdV-Ds closest to each of the 12 sections of the seven HAdV strains is shown in Table 2. The analyses revealed that the closest HAdV type for our seven HAdV strains was different for each section due to frequent recombination events. In section 1, only 890357C was clustered with HAdV-37. In section 5, which includes the region encoding the loops of the hexon gene, all seven of our HAdV strains formed a cluster that was closely related to HAdV-22. In contrast, in sections 3, 4, 6 and 7, which include the regions encoding the penton base gene and C4 of the hexon gene, the four HAdV-53 strains, but not the other three HAdV strains, were clustered with HAdV-37. In sections 11 and 12, which include the fiber gene, 870006C and 880249C were clustered with HAdV-37, whereas 890357C and the four HAdV-53s were closely related to HAdV-8. In all other sections, the seven HAdV strains did not cluster with any of the other 12 HAdV-D strains, and the closest HAdV types could not be detected.

DISCUSSION

HAdV recombination can occur within the same species more readily than between species, and several intermediate recombinant HAdVs have been reported (Adrian *et al.*, 1985; Noda *et al.*, 1991; Engelmann *et al.*, 2006; Aoki *et al.*, 2008; Lukashev *et al.*, 2008; Kaneko *et al.*, 2009, 2011b; Walsh *et al.*, 2009, 2010; Yang *et al.*, 2009). Previous reports have already demonstrated the characteristics of the HAdV-53 genome by recombination among HAdV-D strains (Engelmann *et al.*, 2006; Aoki *et al.*, 2008; Walsh *et al.*, 2009). The identities of the complete genome sequences of all four HAdV-53 strains in this study were high, and the strains formed a single phylogenetic cluster. We compared the complete genome sequences of HAdV-53 strains isolated in Germany with those from Japan (data not shown) and found that all HAdV-53 strains, including those from Germany, formed a single phylogenetic cluster showing high identities (>99.17 %). Thus, it was confirmed that all strains were the same HAdV type, HAdV-53. The identities of the complete genome sequences of the German and Japanese HAdV-53 strains were high (99.17–99.24 %) but were slightly lower than the identities among the Japanese HAdV-53 strains (99.87–100.00 %). The FS161 and FS165 strains, which were isolated in Fukui, were closer to the German strains than the other two Japanese HAdV-53 strains.

In contrast, analyses of the complete genome sequences of three intermediate HAdVs isolated in the 1980s revealed that these did not form a single cluster with the four HAdV-53 strains and showed only low nucleotide sequence identities. The three HAdV strains isolated in the 1980s were neutralized by HAdV-22 antisera (Noda *et al.*, 1991) and showed high nucleotide sequence identity with HAdV-22 at the loop regions in the hexon gene, as observed in the HAdV-53 strains. The identity of the E3 region in these strains and the HAdV-53 strains was also high; however, the three HAdVs from the 1980s did not show hexon-chimeric structures similar to those of HAdV-22 and -37, or a penton base structure similar to that of HAdV-37. Moreover, 87006C and 880249C showed a fiber structure comparable to that of HAdV-37 but not to that of HAdV-8. These three HAdV strains were HAdV-53-like intermediate viruses, but were not HAdV-53. We propose that the 870006C/880249C and 890357C strains are intermediate to HAdV-22/H37 and -22/H8, respectively. Eight HAdV-22/H8 and seven HAdV-22/H37 strains were detected in Japan prior to 1989. However, none of these strains has been isolated since 1990. Many HAdV-53 strains have been isolated from EKC samples since 1996 (Aoki *et al.*, 2011; Kaneko *et al.*, 2011a), suggesting that HAdV-53 evolved from the intermediate HAdVs circulating in the 1980s, and from HAdV-8, -22 and -37, by recombination of sections cut at the putative breakpoints. The origins of the regions for which the HAdV type could not be detected are unknown (Table 2). These sequences might be unique to HAdV-53.

HAdV-53 is serologically related to HAdV-22, which rarely causes EKC. However, HAdV-53 has recently caused epidemic and nosocomial EKC infections in Japan (Kaneko *et al.*, 2011a). It also caused an EKC outbreak in Germany in 2005 (Engelmann *et al.*, 2006). An *in vivo* experiment has shown that HAdV-53, but not HAdV-22, can induce corneal inflammation in a mouse model of corneal infection (Walsh *et al.*, 2009). HAdV-53 obtained its fiber gene, which contains functions related to cell tropism, from HAdV-8 by recombination. Two intermediate HAdV strains isolated in the 1980s, HAdV-22/H37 and -22/H8, also contained the fiber gene from HAdV-37 or -8, respectively, which are the main aetiological agents of

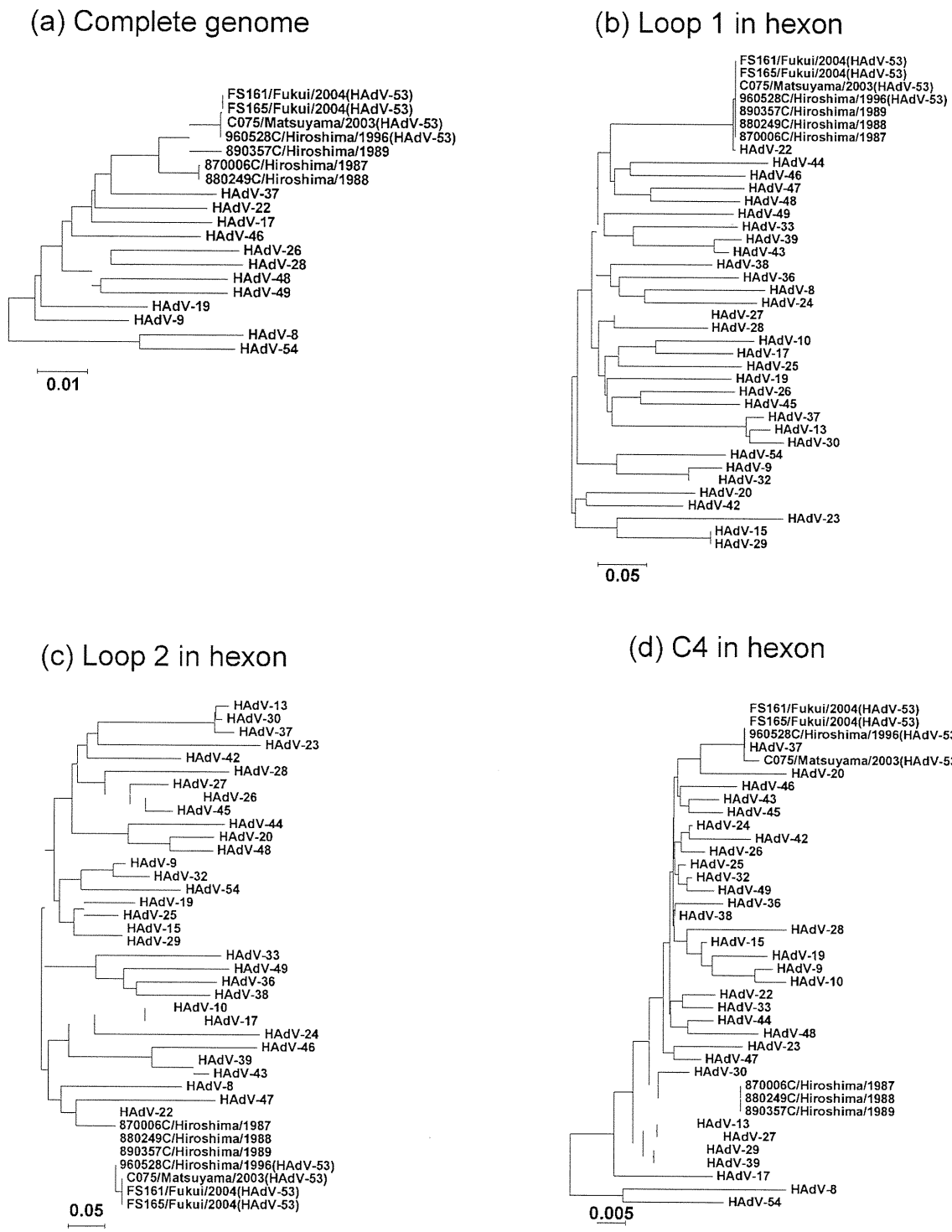

Fig. 2. Phylogenetic analysis of the nucleotide sequences of the complete genome (a), loop 1 (b), loop 2 (c) and C4 (d) in the hexon gene, the penton base gene (e), the E3 region (f) and the fiber gene (g).

EKC. These intermediate strains were isolated between 1986 and 1989 in Japan but did not cause EKC epidemics. HAdV-53 obtained not only the fiber gene from HAdV-8 but also the penton base gene, which is related to cell entry, from HAdV-37 by recombination. This combination of recombination events is thought to have afforded HAdV-53 the ability to infect the eye easily, leading to conjunctivitis.

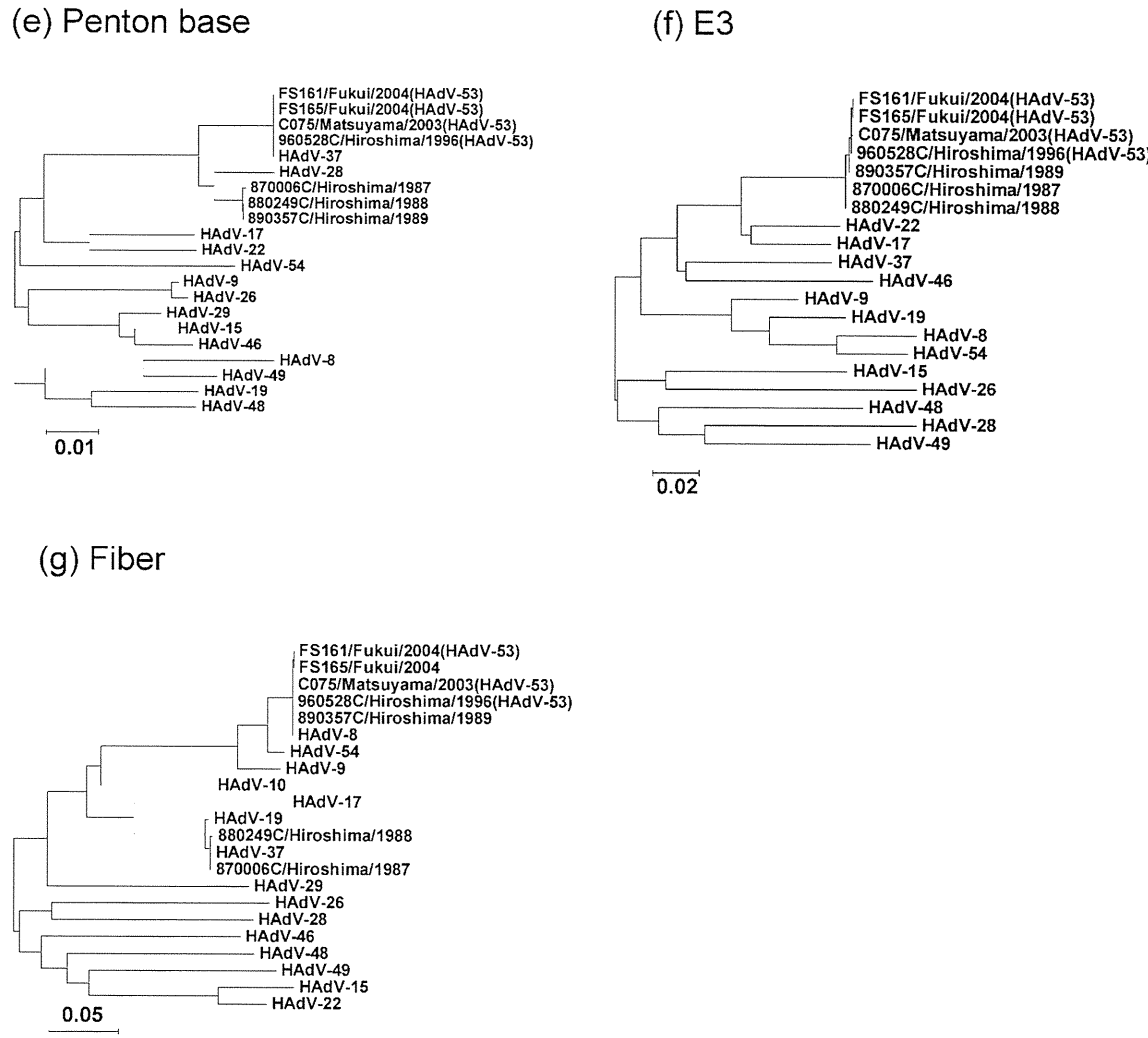

Table 2. HAdV type on the basis of phylogenetic analysis of 12 sections cut at the putative recombinant breakpoints

ND, Not detected.

Section (nt position*)	Closest HAdV type by phylogenetic analysis		
	870006C/880249C	890357C	HAdV-53
1 (1–4311)	ND	HAdV-37	ND
2 (4312–11146)	ND	ND	ND
3 (11201–16151)	ND	ND	HAdV-37
4 (16390–18181)	HAdV-22	HAdV-22	HAdV-37
5 (18182–19357)	HAdV-22	HAdV-22	HAdV-22
6 (19581–21371)	ND	ND	HAdV-37
7 (21372–26447)	ND	ND	HAdV-37
8 (26448–28608)	ND	ND	ND
9 (28609–30091)	ND	ND	ND
10 (30092–31117)	ND	HAdV-8	HAdV-8
11 (31118–32189)	HAdV-37	HAdV-8	HAdV-8
12 (32190–35050)	HAdV-37	HAdV-8	HAdV-8

*The numbering of the positions of the 12 sections corresponds to that of the total sequence of C075/Matsuyama/2003 (HAdV-53).

In conclusion, the complete genome sequence analyses suggested not only the genome organization but also the putative recombination breakpoints and evolutionary processes of the intermediate HAdV-53. Novel HAdVs, including intermediate HAdVs, often cause disease epidemics (Jones *et al.*, 2007; Aoki *et al.*, 2008; Ishiko & Aoki, 2009; Yang *et al.*, 2009; Kaneko *et al.*, 2011a, b). Analyses of both the genes and recombination events in the genome might help predict the appearance of novel HAdVs and disclose the relationships between novel HAdVs and epidemics in the future.

METHODS

Virus strains. Seven clinical intermediate HAdV strains, obtained from EKC patients in Japan, were used in this study (Table 1). Four strains, 870006C, 880249C, 890357C and 960528C, were collected in Hiroshima in 1987, 1988, 1989 and 1996, respectively. The C075 strain was collected in Matsuyama in 2003, and both FS161 and FS165 strains were collected in Fukui in 2004. The strains 870006C/880249C and 890357C were identified previously as HAdV-22/H10,19,37 and HAdV-22/H8,9, respectively, on the basis of NT and HI tests (Noda *et al.*, 1991), whilst the remaining four strains, 960528C, C075, FS161 and FS165, were reported as HAdV-53 on the basis of sequence analyses of the entire hexon and fiber genes (Aoki & Tagawa, 2002; Kaneko *et al.*, 2011a). Viral isolation was propagated in A549 cells. Cell cultures were maintained in Dulbecco's modified Eagle's medium containing 50 μg gentamicin ml^{-1}, 0.5 μg fungizone ml^{-1} and 10 % FCS.

DNA extraction. Viral DNA was extracted from 100 μl of each virus solution using a QIAamp DNA Mini kit (Qiagen) according to the manufacturer's instructions. The extracted DNA was then suspended in 100 μl TE buffer [10 mM Tris/HCl (pH 8.0), 1 mM EDTA].

DNA sequencing. We sequenced the complete genome of HAdV using a PCR/direct sequencing method, as described previously (Kaneko *et al.*, 2009). The primers for PCR and sequencing were designed with reference to the complete genome sequences of other previously deposited HAdV-D strains in GenBank. PCR amplification was performed in 50 μl reaction mixtures containing 10 mM Tris/HCl (pH 8.2), 50 mM KCl, 1.5 mM $MgCl_2$, 200 μM each dNTP, 500 nM each primer and 0.5 U *Taq* DNA polymerase. PCR products were purified with a QIAquick PCR purification kit (Qiagen) and used as templates for DNA sequencing reactions (Kaneko *et al.*, 2005). To determine the sequences of both ends of the genome of each strain, we extracted whole viral DNA from HAdV-infected cells (Shinagawa *et al.*, 1983) and performed a sequencing reaction using the extracted viral DNA as template (Kaneko *et al.*, 2009). Nucleotide sequencing was performed using an autosequencer (ABI Prism 3100 Genetic Analyzer) and a commercial kit (BigDye; Applied Biosystems). The nucleotide sequences were determined on both strands of the amplicons by sequencing to a mean value of greater than threefold coverage of the target regions.

Sequence analysis. Multiple alignments were performed and analysed using CLUSTAL W software (Thompson *et al.*, 1994). Unrooted phylogenetic trees were constructed using the neighbour-joining (NJ) method, and visualized and edited using MEGA4 software (Saitou & Nei, 1987; Walsh *et al.*, 2009). The evolutionary distances were estimated using the Kimura two-parameter method (Kimura, 1980), and unrooted phylogenetic trees were constructed using the NJ method (Saitou & Nei, 1987). Bootstrap analyses were performed with 1000 resamplings of the datasets (Felsenstein, 1985). Similarity plot analyses were generated using SimPlot version 3.5.1 (Lole *et al.*, 1999). Similarities among the complete genomes of the HAdV-D strains were calculated in each window of 200 nt by the Kimura two-parameter method (Kimura, 1980) with a transition : transversion ratio of 2.0. The window was advanced successively along the genome alignment in 20 nt increments.

Identification of putative recombination breakpoints and phylogenetic analysis of each section. To identify recombination breakpoints, the multiple-alignment results were input into the Recombination Detection Program (RDP) (Martin *et al.*, 2005b), which simultaneously applied the following algorithms: RDP (Martin & Rybicki, 2000), Chimaera (Posada & Crandall, 2001), Bootscan (Martin *et al.*, 2005a), GENECONV (Padidam *et al.*, 1999), MaxChi (Smith, 1992) and SiScan (Gibbs *et al.*, 2000). It was used for the complete genome sequences of the seven HAdV strains in this study and 12 HAdV-D strains from GenBank. For the RDP algorithm, the reference sequence parameter was 'Internal and External References', as recommended in the manual, based on the fact that some of the sequences were closely related, whereas others were less closely related. The multiple-aligned sequences were cut into sections at the positions where the putative recombination breakpoints were identified. Among these, sections >1000 bp in length were identified and phylogenetic analyses were carried out by MEGA4 (Tamura *et al.*, 2007). Shorter sections of <1000 bp in length were excluded from the analyses.

Nucleotide sequence accession numbers. The following complete genome HAdV-D sequences, already available in GenBank, were used: HAdV-8 (AB448767), -9 (AJ854486), -17 (AF108105), -19 (AB448771), -22 (FJ404771), -26 (EF153474), -28 (FJ824826), -37 (AB448775), -46 (AY875648), -48 (EF153473), -49 (DQ393829) and -54 (AB448770).

ACKNOWLEDGEMENTS

This work was supported by a Grant-in-Aid for Scientific Research on Innovative Areas from the Ministry of Education, Culture, Sports, Science and Technology of Japan (no. 22125009).

REFERENCES

Adrian, T., Bastian, B., Benoist, W., Hierholzer, J. C. & Wigand, R. (1985). Characterization of adenovirus 15/H9 intermediate strains. *Intervirology* **23**, 15–22.

Aoki, K. & Tagawa, Y. (2002). A twenty-one year surveillance of adenoviral conjunctivitis in Sapporo, Japan. *Int Ophthalmol Clin* **42**, 49–54.

Aoki, K., Ishiko, H., Konno, T., Shimada, Y., Hayashi, A., Kaneko, H., Ohguchi, T., Tagawa, Y., Ohno, S. & Yamazaki, S. (2008). Epidemic keratoconjunctivitis due to the novel hexon-chimeric-intermediate 22,37/H8 human adenovirus. *J Clin Microbiol* **46**, 3259–3269.

Aoki, K., Kaneko, H., Kitaichi, N., Ohguchi, T., Tagawa, Y. & Ohno, S. (2011). Clinical features of adenoviral conjunctivitis at the early stage of infection. *Jpn J Ophthalmol* **55**, 11–15.

Benko, M., Harrach, B., Both, G. W., Russell, W. C., Adair, B. M., Adam, E., de Jong, J. C., Hess, M., Johnson, M. & other authors (2005). Family Adenoviridae. In *Virus Taxonomy: Eighth Report of the International Committee on Taxonomy of Viruses*, pp. 213–228. Edited by C. M. Fauquet, M. A. Mayo, J. Maniloff, U. Desselberger & L. A. Ball. San Diego, CA: Elsevier Academic Press.

Engelmann, I., Madisch, I., Pommer, H. & Heim, A. (2006). An outbreak of epidemic keratoconjunctivitis caused by a new intermediate